Experimental Verification of Magnetic Bearing System Rotordynamics Code

Michal Urednicek
Revolve Technologies Inc., Calgary, Alberta; e-mail: murednic@mail.revolve.com

Clayton Bear
Revolve Technologies Inc., Calgary, Alberta; e-mail: cbear@mail.revolve.com

Abstract: Modeling of magnetically levitated rotors presents unique challenges to the rotordynamicist. The active control system means that bearing characteristics cannot simply be modeled as stiffness and damping coefficients. They must be modeled as closed loop systems that include all elements of the control system as well as the physical characteristics of the shaft. This technique is important in order to properly identify the system to determine appropriate tuning parameter values. Of equal importance is the modeling of the physical shaft including such items as the radial rotors which can be complex laminated sleeves. The impact of these sleeves on the overall rotordynamics can be substantial, especially in smaller shafts where the relative mass of the rotors is high. This paper describes our experience with experimental verification of the accuracy of the model. Three case studies are presented for three substantially different equipment types. Gyroscopic effects and control system interaction with higher order bending modes are also considered.

1.0 Introduction

Rotordynamic analysis represents an important phase of rotating equipment design. When magnetic bearings are used, additional modeling challenges arise from sensor/actuator non collocation and frequency-dependent stiffness and damping characteristics. As a minimum, these characteristics must be included in any meaningful rotordynamic model. Further complexity can be added by accounting for effects of digital control, internal shaft damping and system nonlinearities, for example. Research in these areas is well documented [1-4] and shall not be discussed in detail here.

The focus of this paper is on demonstrating the practical utility of a finite element-based rotordynamic analysis code including an active magnetic bearing control system, in achieving the design objectives in three substantially different machines; a university laboratory test rig, a vacuum compressor, and a six stage centrifugal compressor. In each case, the analysis involved prediction and experimental verification of rotor undamped lateral response, system stability, and unbalance response. The bulk of the discussion will be dedicated to the analysis of the vacuum compressor and six stage centrifugal compressor.

In an effort to keep the controller models as intuitively meaningful as possible, they were treated as analog proportional-integral-derivative (PID) controllers with additional filtering capability (lead-lag networks and notch filters). Rotor models comprised Timoshenko beam segments and solutions included effects of gyroscopic coupling.

The success of each model was measured in terms of its ability to approximately predict basic (PID) tuning parameters based on a reasonably accurate undamped model. A reasonably accurate undamped model response was deemed to be one which agreed with impact measurements (mode shapes and natural frequencies) to within about 15%. In other words, we attempted to determine the level of accuracy required at the undamped model phase to provide the analyst with confidence in the subsequent stability model. Design objectives, system models, and verification are discussed in Section 3.

Another important aspect in the design of a magnetic bearing-equipped system is the placement and design of the auxiliary rundown bearings. This presents a formidable modeling challenge due to the transient, nonlinear nature of the problem. Although detailed modeling of a de-levitation event was beyond the scope of the present work, in Section 3.3.2.3, we discuss a grossly simplified, steady state model found to be useful in determining the most favourable combination of auxiliary bearing location, stiffness, and damping for the six stage compressor. Some static de-levitation test data are presented.

2.0 Analysis Code

A detailed description of the code structure was the topic of an earlier paper [5] so only a brief description shall be provided here.

The analysis code consists of three program segments; undamped critical speeds, system stability, and unbalance response. The shaft is modeled as a series of Timoshenko beam segments. Any added masses (disks, sleeves, etc.) are treated as rigid bodies. Magnetic bearing actuator forces can act over multiple nodes with the control system defined by a ratio of polynomials. In the current version of the code, the full model order is retained, but only steady state lateral mode solutions are considered.

In modeling the shaft's response on auxiliary bearings, only the steady state solution was considered. The bearing stiffness and damping characteristics were

approximated by a proportional-derivative (PD) control transfer function.

3.0 Case Histories

3.1 Case 1: University Test Rig

This system was designed for a vibration analysis group. The shaft is 1600 mm long with a uniform diameter of 39.5 mm. The auxiliary landing system comprises rolling element bearings with elastomer damping rings. This design will be discussed in more detail in Section 3.3.2.3.

3.1.1 Design Objectives

The design criteria for this test rig were; (i) readily adjustable bearing span, (ii) at least one bending mode under 10,000 rpm, (iii) easily accessible mid span and stators, and (iv) variable speed drive with maximum operating speed of 10,000 rpm.

3.1.2 Modeling & Verification

A near maximum bearing span was chosen for the purposes of rotordynamic modeling as this represented a configuration that would exhibit a first bending mode well below 10,000 rpm. The shaft assembly model consisted of 31 segments. The flexible disk coupling was modeled as added mass only, but the bearing rotors were assumed to provide additional stiffness up to the clamping diameter (Figure 1).

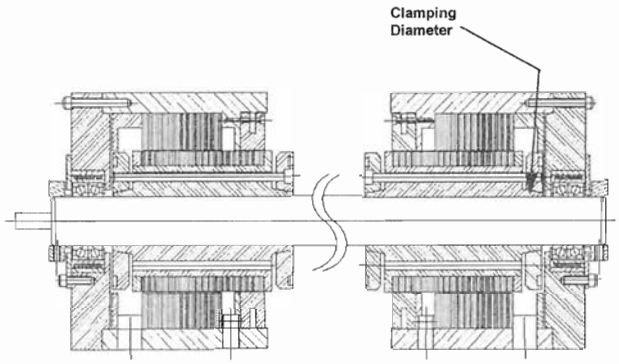

Figure 1. Shaft assembly of university test rig

Figure 2 compares predicted and measured undamped natural frequencies and mode shapes. Note that the predicted natural frequencies are several percent lower than those measured. By contrast, the theoretical mode shapes are in excellent agreement with measured ones. The relatively large discrepancy between predicted and measured natural frequencies is likely due to a slight change in bearing span between measurements as the rotors were repeatedly removed and re-installed. In spite of these discrepancies, we were able to predict the PID gains required to initially levitate the shaft. Fine tuning then proceeded very quickly as two notch filters and a lead-lag filter were added.

The first mode at about 65 Hz appeared difficult to stabilize due to the relative location of the nodes, actuators, and sensors. This was confirmed in the stability model, but was not observed in practice. We believe the coupling added sufficient damping to stabilize this mode. Other instabilities were predicted at 787 and 930 Hz with a severely underdamped mode appearing at 571 Hz. In practice, narrow notch filters were used at 532 and 785 Hz to eliminate these instabilities.

Detailed unbalance response analysis was not performed as the final bearing configuration was unknown.

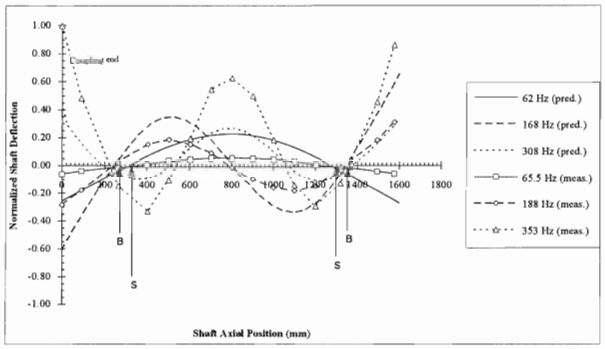

Figure 2. Predicted and measured free-free response

3.2 Case 2: High Speed Vacuum Compressor

The compressor selected for this project was a 5 kW integral motor driven centrifugal compressor, vertically mounted, with a maximum operating speed of 38,500 rpm. It is used in part of a cycle to convert ocean thermal energy to electrical energy by expanding warm surface water into steam, and using this steam to drive a turbine. The plant is a pilot project operated by The Pacific International Center For High Technology Research (PICHTR) in Hawaii.

One of the requirements of the cycle is to remove non condensable gases that evolve out of the ocean water during the expansion phase. Five stages of compression are used to attain the required vacuum. Four of these stages use single stage centrifugal compressors. The fifth is a positive displacement compressor. This project involved the third stage compressor that was experiencing bearing reliability problems. The original bearing configuration consisted of spring loaded precision angular contact bearings mounted on each end of the motor rotor, with an overhung impeller. The intent was to convert the compressor to magnetic bearings.

3.2.1 Design Process

As a first step in the design process in applying magnetic bearings, an estimation of the forces on the rotor is required, both in the radial and axial direction. This is not an easy process, since the forces on a rotor are not generally well known. Static, dynamic, and process fluid forces must all be considered. The dynamic forces can originate from a variety of sources including imbalance, external disturbances, or in this case electrical imbalance from the motor. If the forces are known the bearings can be sized such that they have the capacity to hold the shaft rigidly in place with all these forces combined. In the case of the PICHTR compressor these forces were not known well

enough to accurately be predicted, and therefore, a conservative estimate was used.

Once this estimation of the force requirements was made, the bearing and rotor layout was undertaken. A conical bearing design was chosen to eliminate the need for a thrust bearing, and a tie bolt was used to hold the bearing and motor rotors together as an assembly. The impeller was held onto the tie bolt independently. With this layout completed, the rotordynamic analysis was initiated.

3.2.2 Rotordynamic Analysis

As a baseline, information on the free-free modes and frequencies was provided by the compressor OEM. Since the majority of the mass on the rotor was due to the motor rotor and the impeller, it was important to get a good approximation of the effective stiffness diameter of each component. A model of the rotor was generated using the in-house code, and the relative contribution of stiffness and mass of the motor rotor and impeller were adjusted until good correlation existed between the model and the measured modes.

The next step was to model the rotor with magnetic bearings. The initial design used conical bearings of equal capacity. A shoulder on the tie bolt was located between the impeller and impeller end bearing. This allowed the bearings and motor to be stacked up together as one assembly, and the impeller mounted independently (Figure 3). Prediction of the bending modes of the shaft was a difficult task since the rotor essentially consisted of three complex laminated sleeves held in compression with the tie bolt, and an overhung impeller.

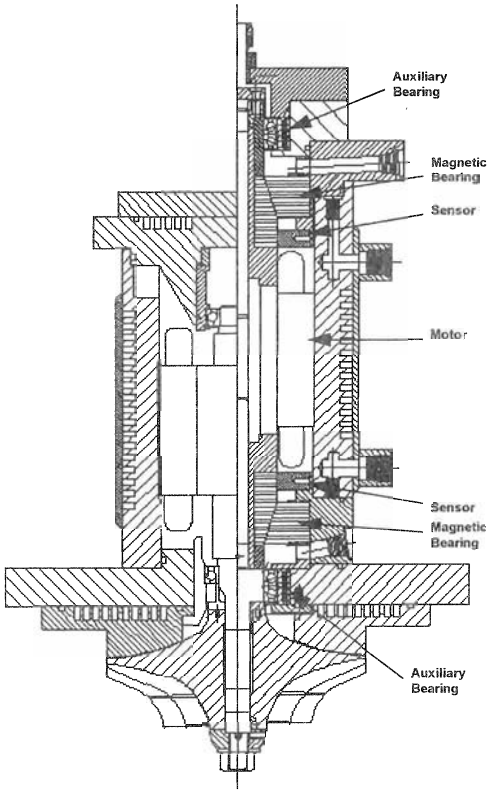

Figure 3. Original layout vs. magnetic bearing layout

In order to get an accurate estimate of each component's contribution to stiffness, an initial set of bearing rotors were built, assembled on the shaft and tested to determine the undamped natural frequencies and mode shapes. The rotordynamic model was adjusted to correlate with the measured frequencies, specifically by adjusting the effective stiffness diameter of each laminated section. It must be noted that great care was taken to ensure good shoulder to shoulder fits between each piece and the tie bolt. Otherwise, the effective stiffness diameter of each piece would be reduced and the corresponding overall shaft stiffness reduced.

Once the model adjustments were completed, a full analysis was undertaken incorporating the active magnetic bearing control system effects. Given the speed of rotation and the relatively large size of the impeller to the shaft, gyroscopic effects were significant. Although our ring tests indicated the first bending mode was at the lower end of the operating range (around 530 Hz, Figure 4), our model predicted the gyroscopic stiffening effect would raise the bending mode frequency to the high end of the operating range (around 600 Hz for the forward whirl mode). It also indicated this mode was poorly damped, meaning operation close to the critical would likely not be possible.

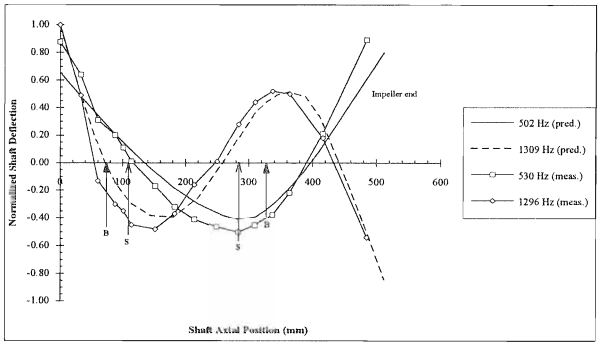

Figure 4. Predicted and measured undamped mode shapes - initial design

Our next step was to verify our model predictions by confirming the location of the mode at speed. These tests confirmed that the mode was in fact where we had predicted, and was poorly damped. This mode would have to be raised in order to attain the desired operating speed range.

3.2.3 Final Design

Analysis of the mode shapes identified that the location on the rotor where changes in geometry would have the greatest impact was on the impeller end bearing. Given the confidence we now had in our rotor dynamics model, we were able to change the design of the rotor until the first bending mode was moved sufficiently out of the operating range.

Several changes were made to the bearing rotor to increase its stiffness contribution. The first was to maximize the lamination inner diameters under the bearing and sensor. This allowed reducing the cone angle of the bearing to

reduce its axial force by the rotor weight to match the axial capacity of the upper bearing. Finally the end ring on the rotor was redesigned to maximize the diameter at which contact was made with the tie bolt shoulder.

The rotor was then reassembled (Figure 5) and a ring test performed. Unexpectedly, the bending mode frequency actually decreased. However, we were able to use the rotordynamics model to predict the observed natural frequencies of the newly fabricated rotor. This analysis identified a manufacturing problem, resulting from improper compression of the laminations, as the cause.

The bearing rotor was then rebuilt, assembled on the compressor rotor and retested. The ring test now showed that the rotor behaved as predicted with these design changes (Figure 6). With the new design change, full speed was attained without exciting the forward whirl mode (Figure 7). Small amplitude swept sine tests were conducted as a final test to locate the critical at speed to confirm the model once more, and verify a reasonable stability margin existed. The tests were successful, and the compressor shipped to site.

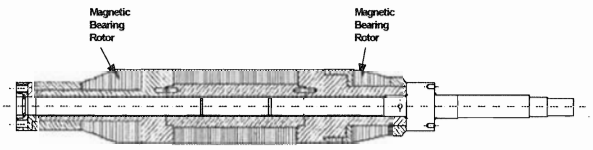

Figure 5. Final rotor layout

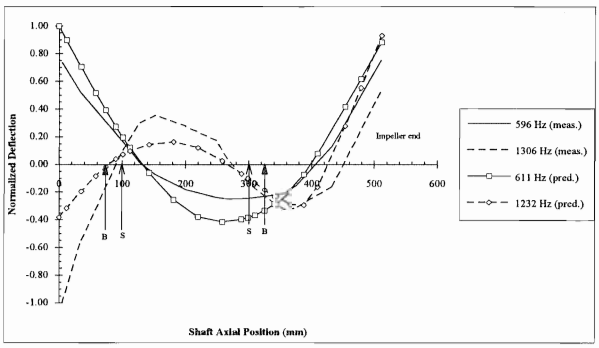

Figure 6. Predicted and measured undamped mode shapes - final design

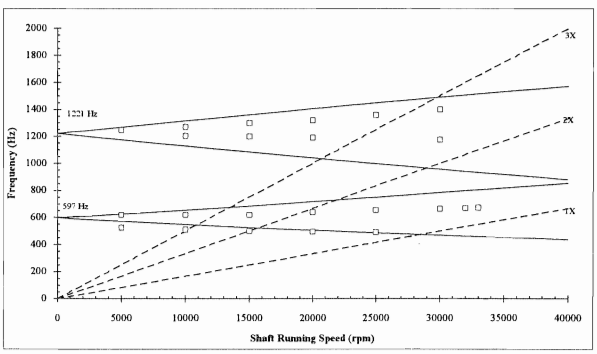

Figure 7. Damped critical speeds - final design (open squares represent observed values)

3.3 Case 3: Six Stage Centrifugal Compressor

This project involved integration of magnetic bearing and dry gas seals into an existing six stage, beam type centrifugal compressor for hydrogen service. The extensive modeling effort was undertaken in three phases. In the preliminary phase, the original shaft assembly was modeled as a baseline and a preliminary magnetic bearing-equipped system model was developed. The intermediate phase involved modeling of numerous magnetic/auxiliary bearing and dry gas seal configurations, and bearing and seal sizing optimizations. The final phase consisted of a complete system model based on the detailed design. This included a steady state analysis of shaft behaviour on auxiliary bearings and prediction of initial tuning parameters.

Once the final design was frozen, a replica of the actual shaft was fabricated and fitted with dummy impellers. This shaft (less any dry seal-related components) was then used for factory commissioning, model verification, and static and dynamic delevitation testing. As this was the only shaft available at the time of this writing, the focus of the following discussion will be on results obtained with it rather than the actual shaft. In Section 3.3.2.1 we present some initial predictions for the actual shaft (seals included) for comparison.

3.3.1 Design Objectives

The retrofit design criteria were as follows:

- Stable operation up to 12,054 rpm
- Satisfaction of API 617 critical speed separation margins; first bending mode at a maximum of 126 Hz (7,611 rpm), and second bending mode at a minimum of 241 Hz (14,465 rpm).
- An auxiliary landing system capable of safely supporting the shaft in the event of delevitation at full speed
- Retention of existing shaft cross-section within the process cavity

3.3.2 Modeling & Verification

3.3.2.1 Final Design Model

The shaft assembly model of the final design is shown in Figure 8. The shaft is almost 2,000 mm long with a maximum mid span diameter of 127 mm. The complete shaft assembly has a mass of approximately 350 kg. All assembly components (diaphragm coupling, sleeves, rotors, etc.) were initially treated as added mass only.

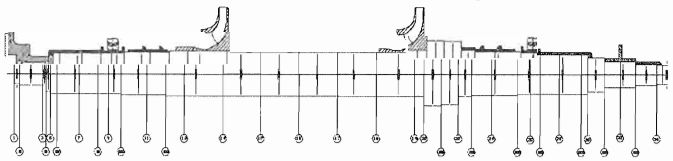

Figure 8. Final design shaft assembly model

The first three free-free natural frequencies were calculated to be 108, 280, and 484 Hz (6,504, 16,800, and 29,043 rpm). In Figure 9, note that the second bending mode, although well outside the operating speed range, is potentially poorly controllable. This was confirmed in the stability model where an analog PID controller was used to stabilize the system (see Figure 10). The 280 Hz mode appeared as stable but highly underdamped. Other poorly damped and unstable modes appeared between 700 and 1500 Hz suggesting a possible need for notch (or other) filters. This will not be confirmed until the completion of on-site commissioning.

The unbalance response analysis employed the same controller model used for the stability analysis. Unbalance masses were calculated using API Standard 617 maximum residual imbalance criteria. Since the results of this analysis will not be physically verifiable until completion of on-site commissioning, we do not present them here. Rather, we discuss the results obtained with the dummy shaft, in the following section.

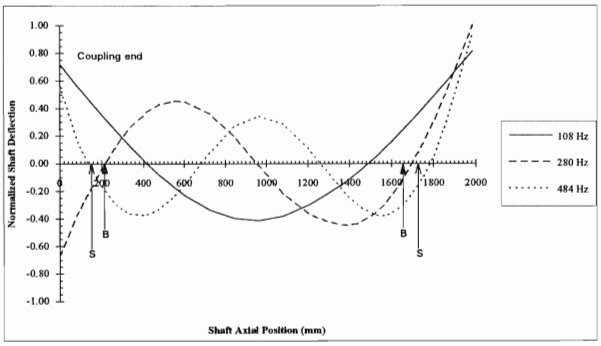

Figure 9. Predicted free-free response

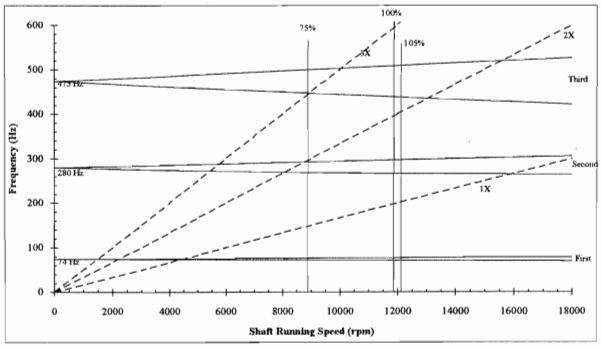

Figure 10. Predicted damped critical speeds

3.3.2.2 Dummy Shaft Model

The dummy shaft model was identical to that used for the final design except for the exclusion of dry seal related masses. The thrust collar was also excluded from the free-free model as it was not installed until we were ready for initial levitation.

Initial predictions of free-free natural frequencies were low when compared with ring test measurements. This suggested that some components were contributing to the shaft stiffness. The most likely stiffness contribution was believed to originate from the impeller span as this region has the tightest interference fits. The modeled effective stiffness diameter was then increased by about 12 mm to match the inter-impeller sleeve outer diameter. Much better agreement between modeled and measured responses was then obtained (Figures 11 and 12).

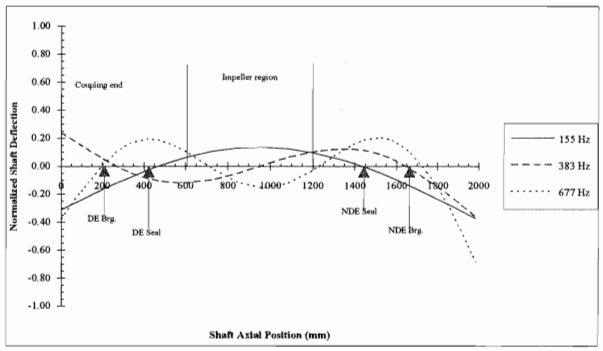

Figure 11. Predicted free-free response (dummy shaft)

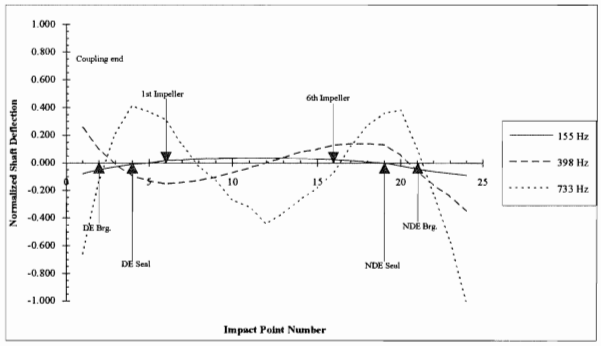

Figure 12. Measured free-free response (dummy shaft)

The thrust collar was then added to the model and PID gains were predicted. It was not possible to stabilize the model until each bearing's force was distributed over the same four nodes over which the rotors' mass was distributed. Interestingly enough, the model remained unstable when the bearing forces were distributed over only three of the rotors' nodes. Although levitation was possible with the predicted gains, the system was only marginally stable. Higher frequency oscillations persisted above 300 Hz so notch filters were implemented and PID gains were adjusted accordingly. This was not entirely surprising as many of the predicted modal frequencies above 200 Hz were poorly damped. Specifically, the predicted mode at 305 Hz had a damping ratio of only 0.005. When tuning, a notch was actually set at 310 Hz, but was required only at the drive end.

The final tuning required four notches at the non drive end, all above 500 Hz, and three notches at the drive end, again all above 500 Hz (except for the 310 Hz notch). It should be noted that in its present form, the model could not be used to accurately predict the placement of notch filters. In fact, when all notch and lowpass filters were included in the system model, instabilities appeared at frequencies which were not observed in the actual system. Table 1 lists the eigenfrequencies predicted for the analog-controlled dummy shaft (using the actual PID gains and a

2kHz lowpass filter) and Figure 13 shows a measured response to a swept sine perturbation.

Predicted System Eigenfrequency (Hz)	Damping Ratio
85	0.091
305	0.005
509	0.095
702	0.254
930	0.492
932	0.357
1175	0.103

Table 1. Predicted system eigenfrequencies.

There is a number of likely contributors to the discrepancies between predicted and measured results. The following are probably some of the more dominant factors:

1. Recall that the diaphragm coupling was modeled as a mass element only, where in fact, it may behave more like another shaft segment with an additional bearing. This is supported by our observations during system tuning where the coupling was found to improve the transmissibility of the higher order modal frequencies, thereby contributing to the onset of self-excited oscillations.
2. When notch filters are used, it is difficult to obtain good agreement between modeled and actual systems as notch filters do not represent a robust filter design method.
3. By modeling the control system as analog, we may be neglecting some important system lags. It is unlikely this is a dominant factor, but it may account for some of the discrepancies.

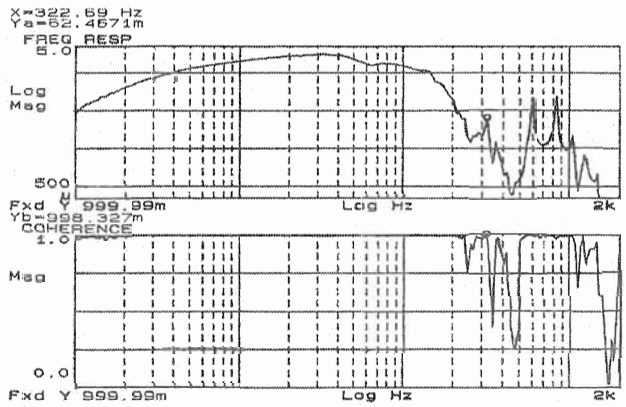

Figure 13. Response of dummy shaft system to swept-sine perturbation.

Again, the unbalance response analysis employed the same controller model used for the stability analysis. Shaft responses for two imbalance cases were modeled and measured; (1) 707 g mm at 0° mid span, and (2) 707 g mm at 0° mid span and 350 g mm at 270° on impeller six. Both responses were modeled and measured at an operating speed of 12,000 rpm. Table 2 lists predicted and measure peak to peak shaft excursions at four sensor locations.

	Predicted Peak-Peak Shaft Excursion (mils)				Measured Peak-Peak Shaft Excursion (mils)			
	Drive End	Mid Span	Non Drive End	Thrust Disk	Drive End	Mid Span	Non Drive End	Thrust Disk
Case 1	0.02	0.40	0.50	0.25	1.5	1.3	0.60	0.80
Case 2	0.56	0.43	0.60	0.28	1.4	1.1	0.60	0.70

Table 2. Predicted and measured peak displacements.

Comparison of predicted and measured values in Table 2 clearly points to some inadequacies in our model, at least for the 12,000 rpm running speed. During testing, some support structure resonances were found to influence the measured orbits. These influences have not been completely isolated yet so a firm conclusion is not possible at this time.

3.3.2.3 Auxiliary bearings

In modeling the shaft response on auxiliary bearings, only shaft whirl was considered; that is, impact mechanics or other transient or nonlinear phenomena were not considered. The response was initially calculated as a function of support stiffness only. Two imbalance cases, believed to represent bad and worst case scenarios, were used to estimate the actual response. The bad case scenario was modeled as a shaft with a 10 x API maximum residual imbalance split between the first and sixth impellers, in phase. In the worst case, the complete shaft assembly mass was used to calculate a dynamic load at the predicted rigid body and first bending mode frequencies for an eccentricity of 8 mils, corresponding to the auxiliary bearing clearance. The calculated dynamic load was then distributed over all shaft nodes. Responses for both scenarios were calculated over a range of support stiffness extending from 5.26e7 to 2.63e8 Nm^{-1}. Shaft excursions were found to be excessively large for both scenarios and modal frequencies.

Referring to work done in previous investigations [6-10], we hoped to reduce the shaft excursions by providing an appropriate combination of support stiffness and damping. Initially, only elastomer-damped rolling element bearings were considered, but further investigation of other damping materials is in progress. Support stiffness and damping was now modeled as a proportional-derivative (PD) controlled magnetic bearing with a collocated position sensor. The bad case scenario was modeled as described above, but the frequency used to calculate the dynamic load was taken to be that of the first rigid mode. In the worst case, the maximum eccentricity was now assumed to be 5 mils, approximating the compressibility of the elastomer damping ring. The use of the first natural frequency for calculating dynamic load is based on results presented in the above-mentioned literature where the authors observed an excitation of the first natural frequency almost immediately after rotor drop. Shaft responses were again calculated for a wide range of stiffness and damping values. The "best" responses, for both scenarios, were calculated at support stiffness and damping values of 2.62e7 Nm^{-1} and 6.16e4 Ns m^{-1}, respectively. Under these conditions, the two rigid modes appeared between about 60 and 70 Hz, and the first bending mode appeared at about 110 Hz.

The predicted bad and worst case responses are shown in Figures 14 and 15.

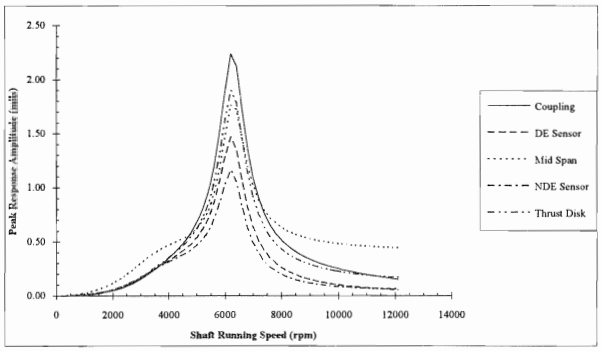

Figure 14. "Bad" case response (10 x API)

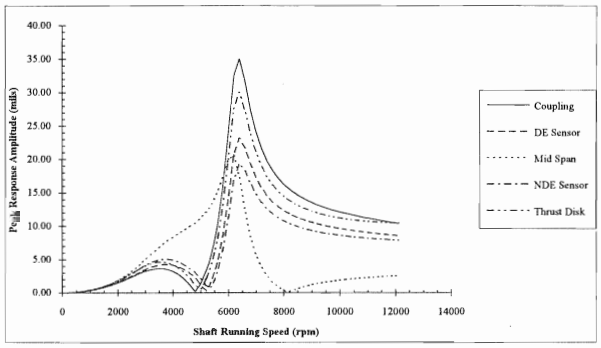

Figure 15. "Worst" case response (full dynamic load)

In the worst case scenario, we see unacceptable shaft excursions only if the ~6,000 rpm mode is excited. Otherwise the responses for both scenarios are well within internal clearances.

A test rig incorporating electromagnetic shakers was then designed to measure stiffness and damping characteristics of various damping ring configurations (This rig will be discussed in more detail in a forthcoming paper dealing with the drop test results). Specifically, it was important to know if the stiffness and damping values used to determine the best responses were physically achievable. The best physically attainable stiffness and damping values were found to be 7.7e7 Nm^{-1} and 1.0e5 Ns m^{-1}. These values were used for the subsequent drop tests. Initially, only static delevitation response was measured. The levitated shaft was released from pre-set air gaps (all axes were released simultaneously) and position was measured at a number of axial locations. As can be seen in Figure 16 , the response was well damped. Based on these results, a decision was made to proceed with dynamic drop tests. The shaft was dropped repeatedly over a range of speeds between 2000 and 12000 rpm, with deflections never exceeding internal clearances. As the dynamic delevitation data is still being reviewed, we cannot yet discuss the delevitation mode shapes. Again, this will be discussed in the forthcoming paper.

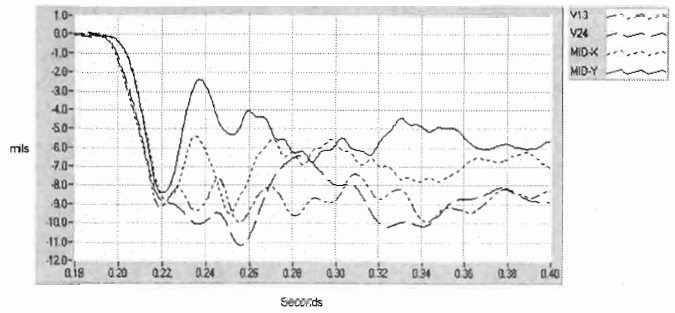

Figure 16. Sample static delevitation response.

4.0 Conclusions

The practical utility of a rotordynamics analysis code was demonstrated through the meeting of design objectives for three vastly different machines.

All predicted undamped natural frequencies were within 15% of measured values. Although this appears to be sufficient accuracy for the purposes of checking effects of mechanical design modifications, component fits, and estimating PID tuning parameters, it is insufficient for detailed stability analysis and optimal control system design. This was shown in the results as some modeled instabilities did not appear in practice.

We also showed how a greatly simplified model was used to determine the most favourable axial position and stiffness and damping characteristics of the auxiliary landing system for a six stage compressor. Dynamic delevitation data are now being analyzed to determine coast down modal behaviour. These results will be presented in a forthcoming paper.

References

[1] E.S. Zorzi, H.D. Nelson, "Finite Element Simulation of Rotor-Bearing Systems with Internal Damping," *ASME Journal of Engineering for Power*, **99(A1)**, p.71-76, (1975).

[2] P.J. Brosens and S.H. Crandall, "Whirling of Unsymmetrical Rotors," *Journal of Applied Mechanics*, **September 1961**, p.355-362.

[3] Y. Okada, et al., "Cross-Feedback Stabilization of the Digitally Controlled Magnetic Bearing," *ASME Journal of Vibration and Acoustics*, **114**, p.54-59, (1992).

[4] K.V. Hebbale, A Theoretical Model for the Study of Nonlinear Dynamics of Magnetic Bearings, Ph.D. Dissertation, Cornell University, January 1985.

[5] E.C. Mikulcik, M. Urednicek, "A Rotordynamic Analysis Code for Digitally Controlled Magnetic Bearings", REVOLVE'93 Conference Proceedings, Calgary, Alberta, June 1994

[6] J.A. Tecza, et al., "Elastomer Mounted Rotors - An Alternative for Smoother Running Turbomachinery," *Transactions of the ASME*, **79-GT-149**, (1979).

[7] A.J. Smalley, M.S. Darlow, and R.K. Mehta, "The Dynamic Characteristics of O-Rings," *Transactions of the ASME*, **100**, p.132-138, (1978).

[8] J.A. Tecza, et al., "Design of Elastomer Dampers for a High-Speed Flexible Rotor," *ASME Publication* **79-DET-88**, September 1979.

[9] F. Alves, and C. Lee, "Dynamic Test of Auxiliary Landing System for Magnetic Bearings (Drop Test)," REVOLVE'92 Conference Proceedings, Calgary, Alberta, April 1992.

[10] T. Ishii, and R. Gordon Kirk, "Analysis of Rotor Drop on Auxiliary Bearings Following AMB Failure," ROMAG'91 Conference Proceedings, Alexandria, Virginia, March 1991.